

Electron Beam Dump Constraints on Light Bosons with Lepton Flavor Violating Couplings

Takeshi Araki,^{1,*} Kento Asai,^{2,†} and Takashi Shimomura^{3,4,‡}

¹*Faculty of Dentistry, Ohu University, 31-1 Sankakudo,
Tomita-machi, Koriyama, Fukushima 963-8611, Japan*

²*Department of Physics, Faculty of Science,
Saitama University, Sakura-ku, Saitama 338-8570, Japan*

³*Faculty of Education, University of Miyazaki,
1-1 Gakuen-Kibanadai-Nishi, Miyazaki 889-2192, Japan*

⁴*Department of Physics, Kyushu University,
744 Motoooka, Nishi-ku, Fukuoka, 819-0395, Japan*

(Dated: July 16, 2021)

Abstract

We study constraints on light and feebly interacting bosons with lepton flavor violation from electron beam dump experiments. Scalar, vector, and dipole interactions of the bosons are analyzed, respectively, and excluded regions from the searches for decays into electron-positron pairs are derived. It is found that parameter regions unconstrained by flavor violating decays of muon can be excluded using the results of the E137 experiment. We also discuss the impact of the search for flavor violating decays of the light bosons in electron beam dump experiments.

* t-araki@den.ohu-u.ac.jp

† asai@krishna.th.phy.saitama-u.ac.jp

‡ shimomura@cc.miyazaki-u.ac.jp

I. INTRODUCTION

For the last decade, the searches for new physics beyond the Standard Model (SM) have been primarily led by the LHC with particular attention to the regions of TeV-scale mass with $\mathcal{O}(1)$ coupling. Despite a great deal of experimental and theoretical efforts has been made in that direction, no signals have been found so far. Given the fact, recently, there is a growing interest in a neutral boson having sub-GeV mass and feeble interactions with the SM particles. In fact, there are several theoretical motivations to consider such a feebly-interacting light boson; For instance, it plays a crucial role in the dark matter problem [1–7], the muon $g - 2$ anomaly [8–10], the Hubble tension [11–14], and it is also claimed that the existence of the light boson helps us understand the observed energy spectrum of high energy cosmic neutrino [15–23].

Feebly-interacting light bosons are expected to be long-lived and leave very displaced vertex signals at experiments. Among possible experiments, beam dump experiments are especially suitable for searching such bosons. The bosons can be created from incoming beam on a target, travel long distance, and decay to electron-positron pairs near the detector distant from the target. In the 1980s, several beam dump experiments were carried out to search for light neutral scalar bosons, such as axions, by using proton beam [24] and electron beam [25–29], and their experimental constraints were later translated to those on gauge bosons in Refs. [30] and [31, 32], respectively. At present, the results of the beam dump experiments have been applied to various types of light boson models, and comprehensive analyses including constraints from collider experiments have also been done, e.g., see Refs. [33], [34, 35], and [36] for the $B - L$ and the $L_\alpha - L_\beta$ gauge boson ($\alpha, \beta = e, \mu, \tau$), the dark photon, and the dark higgs boson, respectively. Also, in Refs. [37–40], the prospect of a new beam dump experiment at the future ILC experiment is studied.

Thought, beam dump experiments are probably the best probe of searching for feebly-interacting light bosons, the constraints are derived by assuming the simplest model setup, that is, only a single particle and a single coupling constant are introduced. In the literature, however, several extensions have been proposed recently.

In this paper, given the current situation, we attempt to enlarge the availability of beam dump experiments for the extended scenarios. We are especially interested in extensions including Charged Lepton Flavor Violation (CLFV) [41–44]. As is well known, CLFV is one of the most evident signals for new physics beyond the SM. Many experimental searches have been carried out, and in most cases muonic processes like $\mu \rightarrow eee$ and $\mu \rightarrow e\gamma$ place the tightest upper bounds on CLFV couplings. On the other hand, in the sub-GeV mass regions, electron beam dump experiments can possibly exclude parameter regions below the upper bounds from the muonic processes, and new bounds could be obtained. To illustrate

the exclusion regions of electron beam dump experiments, we consider three benchmark scenarios for a new light boson, i.e., a scalar boson having Yukawa interactions, a gauge boson having vectorial interactions, and a gauge boson having dipole interactions. For these, we introduce CLFV couplings in the electron (e) and muon (μ) sector as well as Charged Lepton Flavor Conserving (CLFC) couplings, and derive the constraints from the E137 experiment, which usually provides the strongest constraints.

This paper is organized as follows. In Sec. II, we introduce three types of CLFV interactions analyzed in this work. In Sec. III, the production cross sections of light bosons through bremsstrahlung processes and the formula to calculate the number of signal events are given. In Sec. IV, the constraints on the light bosons with CLFV coupling by the E137 experiment are derived, and the results are compared with the existing bounds from the muon CLFV decays. In Sec. V, the impact of searches for flavor violating decays are discussed. Section VI is devoted to summary.

II. INTERACTION LAGRANGIAN

We start our discussion by introducing interaction Lagrangians analyzed in this work. We consider three types of interactions, i.e., scalar-, vector- and dipole-type interactions, and briefly discuss the origin of these interactions in mind a two Higgs doublet model, a gauged $L_\mu - L_\tau$ model [45–47] and a dark photon model, respectively. In the following, we restrict our analyses only to CLFC and CLFV in the $e\mu$ sector.

A. Scalar interactions in two Higgs doublet model

Firstly, we give the scalar-type interaction Lagrangian. Such an interaction can be obtained in models with an extra leptophilic Higgs doublet scalar. The new Higgs doublet scalar is assumed to couple to only leptons and to contribute to mass generation of the charged leptons. In this case, the mass matrix of the charged leptons consists of two parts originating from each Higgs doublet after developing vacuum expectation values (VEVs). In general, those two mass matrices are not necessarily diagonalized simultaneously, and the misalignment of the mass matrices generates CLFV interactions after the diagonalization. To avoid large contributions from the CLFV interaction by the SM Higgs boson, we assume the VEV of the extra Higgs doublet field to be much smaller than the electroweak scale. Then, the charged lepton masses are mostly determined by mass matrix with the VEV of the SM Higgs boson. In such a case, the CLFV interactions are given from the Yukawa terms of the extra scalar boson.

The relevant interaction Lagrangian is given by

$$\mathcal{L}_{\text{scalar}} = \sum_{\ell=e,\mu,\tau} y_\ell \bar{\ell}_L \phi \ell_R + y'_{e\mu} \bar{e}_L \phi \mu_R + y'_{\mu e} \bar{\mu}_L \phi e_R + h.c. , \quad (1)$$

where ϕ is the extra scalar boson, and y_ℓ and $y'_{e\mu(\mu e)}$ are the CLFC and CLFV coupling constants, respectively. Here we omit the interactions obtained from the mixing between ϕ and the SM Higgs boson, due to the assumption of a small VEV for ϕ .

From Eq. (1), the total decay width of ϕ is given by

$$\Gamma_{\text{tot}} = \sum_{\ell=e,\mu,\tau} \Gamma(\phi \rightarrow \ell \bar{\ell}) + \Gamma(\phi \rightarrow e \bar{\mu}) + \Gamma(\phi \rightarrow \mu \bar{e}) . \quad (2)$$

Here the partial decay widths into the charged leptons are given by [48, 49]

$$\Gamma(\phi \rightarrow \ell \bar{\ell}') = \frac{S^2}{8\pi} m_\phi \left[1 - \frac{(m_\ell + m_{\ell'})^2}{m_\phi^2} \right]^{3/2} \sqrt{1 - \frac{(m_\ell - m_{\ell'})^2}{m_\phi^2}} , \quad (3)$$

where $S = y_\ell$ or $y'_{e\mu(\mu e)}$ for the CLFC- and CLFV-decays, respectively.

B. Vector interactions in $L_\mu - L_\tau$ model

Next, we give the vector-type interaction Lagrangian. The interactions of the charged leptons with a new vector boson can be obtained by extending the gauge sector of the SM. For minimality, we consider an extra U(1) gauge symmetry in this work. CLFV vector interactions can be generated at both tree and loop levels. At tree level, the following conditions should be satisfied: 1) the different gauge charge assignments among charged lepton flavors, and 2) the misalignment between the interaction and mass eigenstates of the charged leptons. Then, CLFV interactions appear in the gauge sector after diagonalizing the mass matrix of the charged leptons. It should be noticed that the above conditions imply that the extra U(1) symmetry must be flavor-dependent. Therefore flavor universal gauge symmetries, such as the $U(1)_{B-L}$ gauge symmetry, can not induce the CLFV interactions in this way. One of the viable examples is the $U(1)_{L_\mu - L_\tau}$ gauge symmetry with extra Higgs doublets. Under the $U(1)_{L_\mu - L_\tau}$ gauge symmetry, the lepton flavors are differently charged: only the mu and the tau leptons (τ) are charged as +1 and -1, respectively. Moreover, if there exist extra Higgs doublets charged under the $U(1)_{L_\mu - L_\tau}$ gauge symmetry, off-diagonal elements in the charged lepton mass matrix are induced [47]. At loop level, CLFV vector interactions will be induced through the CLFV scalar loop for massive gauge bosons. In this case, it is unnecessary for the gauge symmetry to be flavor-dependent. In this work, we only study the CLFV vector interactions at the tree level. However, analyses for the

loop-induced CLFV interactions are essentially the same and will be translated by replacing the couplings with loop-induced ones in our results.

For general discussions, we parametrize the CLFV coupling by θ which is the mixing angle between electron and muon. The mass and flavor eigenstates are connected by this mixing angle. Then, the Lagrangian of the vector interaction in mass eigenstate is given by

$$\begin{aligned} \mathcal{L}_{\text{vector}} = & g' Z'_\rho (s^2 \bar{e} \gamma^\rho e + c^2 \bar{\mu} \gamma^\rho \mu + sc \bar{\mu} \gamma^\rho e + sc \bar{e} \gamma^\rho \mu) \\ & + g' Z'_\rho (-\bar{\tau} \gamma^\rho \tau + \bar{\nu}_\mu \gamma^\rho \nu_\mu - \bar{\nu}_\tau \gamma^\rho \nu_\tau) , \end{aligned} \quad (4)$$

where Z' is the gauge boson and g' is the gauge coupling constant of the $U(1)_{L_\mu-L_\tau}$ gauge symmetry, and $s = \sin \theta$ and $c = \cos \theta$, respectively. Here ν_μ and ν_τ are left-handed muon and tau neutrinos. It should be noted that, in general, there also can exist interactions through the kinetic mixing. Such interactions conserve lepton flavor and are independent of the mixing angle. Then, the flavor conserving productions and decays of Z' are modified. Although analyses of such a situation will lead more general constraints, the increase of the parameters will make the analyses complicated. For simplicity, we assume that contributions from the kinetic mixing can be negligible, and omit the kinetic mixing throughout this paper.

Given the Lagrangian in Eq. (4), the total decay width of Z' is obtained as

$$\Gamma_{\text{total}} = \Gamma(Z' \rightarrow \nu\bar{\nu}) + \sum_{\ell=e,\mu,\tau} \Gamma(Z' \rightarrow \ell\bar{\ell}) + \Gamma(Z' \rightarrow e\bar{\mu}) + \Gamma(Z' \rightarrow \mu\bar{e}) , \quad (5)$$

where the partial decay width into the neutrinos is given by

$$\Gamma(Z' \rightarrow \nu\bar{\nu}) = \frac{g'^2}{12\pi} m_{Z'} , \quad (6)$$

in the limit of massless neutrinos¹, while those into the charged leptons are

$$\begin{aligned} \Gamma(Z' \rightarrow \ell\bar{\ell}') = & \frac{V^2}{24\pi} m_{Z'} \lambda \left(\frac{m_\ell^2}{m_{Z'}^2}, \frac{m_{\ell'}^2}{m_{Z'}^2} \right) \\ & \times \left[2 - \frac{m_\ell^2 - 6m_\ell m_{\ell'} + m_{\ell'}^2}{m_{Z'}^2} - \frac{(m_\ell^2 - m_{\ell'}^2)^2}{m_{Z'}^4} \right] , \end{aligned} \quad (7)$$

where $V = g's^2$ ($g'c^2$) or $g'sc$ for the decays into ee ($\mu\mu$) or $e\bar{\mu}$ and $\bar{e}\mu$, respectively, and $\lambda(a, b)$ is the Kallen function defined as follows :

$$\lambda(a, b) = \sqrt{1 + a^2 + b^2 - 2a - 2b - 2ab} . \quad (8)$$

¹ Here we assumed neutrinos are Dirac particle. For Majorana neutrinos, the partial decay width is multiplied by 1/2.

C. Dipole CLFV in Dark Photon Model

Lastly, we give the dipole-type interaction Lagrangian. We again consider an extra U(1) gauge symmetry and assume that there are no interactions between the new gauge boson A' and the SM particles at tree level, similar to the dark photon model with vanishing kinetic mixing. Even in this case, CLFV interactions, as well as CLFC interactions, can be induced at the loop level. For instance, suppose new complex scalar bosons charged under the extra symmetry exist and couple to the SM charged leptons with new fermions. The interaction between A' and charged leptons can be generated at one-loop in which the new scalar bosons and fermions propagate. Here we consider the following dipole-type interactions:

$$\mathcal{L}_{\text{dipole}} = \frac{1}{2} \sum_{\ell=e,\mu,\tau} \mu_\ell \bar{\ell} \sigma^{\rho\sigma} \ell A'_{\rho\sigma} + \frac{\mu'}{2} (\bar{\mu} \sigma^{\rho\sigma} e + \bar{e} \sigma^{\rho\sigma} \mu) A'_{\rho\sigma}, \quad (9)$$

where μ_ℓ and μ' are CLFC and CLFV dipole couplings, respectively, and $A'_{\rho\sigma}$ stands for the field strength of A' . We assume that the dipole couplings are real. One may imagine that there should exist similar CLFV interactions in which external A' is replaced by photon, which are strictly constrained by the MEG [50] and BaBar [51] experiments. However, it will be possible to suppress such dangerous electromagnetic dipole operators when the new gauge boson has an interaction vertex with neutral CP-even and odd scalars since the same vertex does not exist for the photon. One of such examples is the so-called dark photon model with dark Higgs particles [52].

Given the Lagrangian in Eq. (9), the total decay width of A' is given by

$$\Gamma_{\text{total}} = \sum_{\ell=e,\mu,\tau} \Gamma(A' \rightarrow \ell\bar{\ell}) + \Gamma(A' \rightarrow e\bar{\mu}) + \Gamma(A' \rightarrow \mu\bar{e}), \quad (10)$$

where

$$\begin{aligned} \Gamma(A' \rightarrow \ell\bar{\ell}') &= \frac{D^2}{12\pi} m_{A'}^3 \lambda \left(\frac{m_\ell^2}{m_{A'}^2}, \frac{m_{\ell'}^2}{m_{A'}^2} \right) \\ &\times \left[\frac{1}{2} + \frac{1}{2} \frac{m_\ell^2 + 6m_\ell m_{\ell'} + m_{\ell'}^2}{m_{A'}^2} - \frac{(m_\ell^2 - m_{\ell'}^2)^2}{m_{A'}^4} \right], \end{aligned} \quad (11)$$

$D = \mu_\ell$ or μ' for CLFC or CLFV decays, respectively, and $\lambda(a, b)$ is given in Eq. (8).

III. SCALAR AND GAUGE BOSON PRODUCTION IN BEAM DUMP EXPERIMENTS

In electron beam dump experiments, a new light boson X ($= \phi, Z', A'$) is produced by the bremsstrahlung process with nucleons in target materials. When the light bosons have CLFV

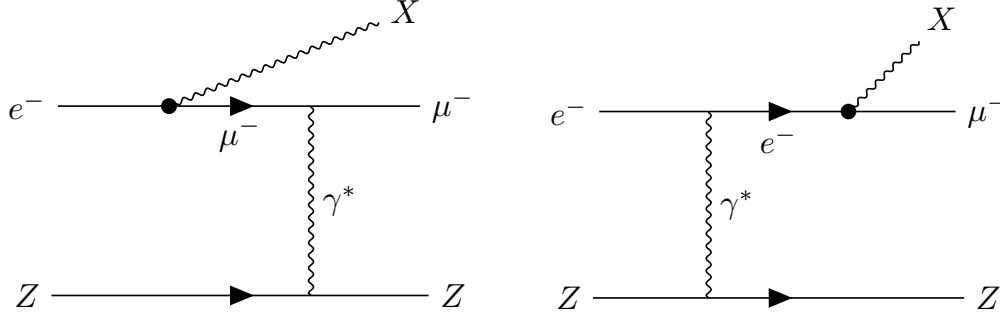


FIG. 1. Light boson production through bremsstrahlung process with CLFV interaction by a target with the atomic number Z .

interactions with electron and muon, they also can be produced through flavor violating bremsstrahlung processes shown in Fig. 1. The bremsstrahlung production process can be evaluated by using the cross section of electron-photon scattering, $e^- + \gamma \rightarrow \ell + X$ ($\ell = e, \mu$), in the Weizsäcker-Williams approximation [53–55]. In this section, we show the differential cross sections of the scalar and vector boson production process for the interactions given in the previous section. Then, we give formulae to calculate the number of events in electron beam dump experiments.

A. Differential cross section of bremsstrahlung process

With the improved Weizsäcker-Williams approximation, the differential cross section of bremsstrahlung process of the light boson production by a target with atomic number Z , $e^- + Z \rightarrow \ell^- + Z + X$ ($\ell = e, \mu$, $X = \phi, Z', A'$), is calculated by that of scattering one, $e^- + \gamma \rightarrow \ell^- + X$, as follows :

$$\frac{d\sigma_{\text{brems}}}{dx} = \frac{\alpha\xi E_0 x \beta_X}{\pi} \frac{d\sigma_{\text{scat}}}{dx}, \quad (12)$$

where α is the electromagnetic fine structure constant, E_0 is the energy of the injected electron beam, $\beta_X = \sqrt{1 - m_X^2/E_e^2}$ is the kinematical factor, and $x = E_X/E_e$ with $E_e(X)$ being the energy of incident electron (produced light boson). The effective photon flux is denoted as ξ [31], and the definition of ξ is given in Appendix A. The differential cross section of the scattering process with respect to x is given by

$$\frac{d\sigma_{\text{scat}}}{dx} = \frac{\alpha g_X^2}{2E_0} \frac{1-x}{x} \left[f_1(x) \frac{\tilde{U}_1^\ell}{m_X^2} + f_2(x) \frac{\tilde{U}_2^\ell}{E_e^2 x} - f_3(x) \left(x \frac{m_X^2 \tilde{U}_3^\ell}{(E_e^2 x)^2} - (1 - a_1 x + r_e x^2) \frac{m_X^4 \tilde{U}_4^\ell}{(E_e^2 x)^3} \right) \right], \quad (13)$$

where g_X and m_X are the coupling constant and mass of the light boson X , respectively. In the square bracket, \tilde{U}_n^ℓ ($n = 1-4$) are functions of the maximal angle θ_{\max} determined by the angular acceptance of the detector and η_ℓ given by

$$\eta_\ell = \frac{m_X^2}{E_e^2} \frac{1-x}{x^2} + \frac{m_e^2}{E_e^2} + \frac{m_\ell^2 - m_e^2}{E_e^2 x}, \quad (14)$$

where m_ℓ is the mass of lepton ℓ . The definition and approximate form of \tilde{U}_n^ℓ are given in Appendix B. The functions $f_1(x)$, $f_2(x)$ and $f_3(x)$ depend on the final state lepton ℓ and the types of the light boson X . For convenience, we define

$$r_\ell = \frac{m_\ell^2}{m_X^2}, \quad (15)$$

and

$$a_1 = 1 + r_e - r_\ell, \quad (16a)$$

$$a_2 = 1 - r_e - r_\ell, \quad (16b)$$

$$a_3 = 2 + r_e + r_\ell - 2\sqrt{r_e r_\ell}, \quad (16c)$$

$$a_4 = 2 - r_e - r_e^2 - r_\ell - r_\ell^2 + 6\sqrt{r_e r_\ell} + 2r_e r_\ell. \quad (16d)$$

Note that $\ell = e$ corresponds to the case of the CLFC interactions while $\ell = \mu$ to the CLFV interactions. Thus, the difference between the CLFC and CLFV interactions arises in the third term of η_ℓ as well as r_ℓ and g_X .

For the scalar interaction given in Eq. (1), $X = \phi$ and $g_\phi = 1$. The functions $f_{1,2,3}(x)$ in Eq. (13) are

$$f_1(x) = 0, \quad f_2(x) = S_1 \frac{x^2}{2}, \quad f_3(x) = (a_2 S_1 - 4\sqrt{r_e r_\ell} S_2)(1-x), \quad (17)$$

where $S_1 = |y_{e\mu}|^2 + |y_{\mu e}|^2$ and $S_2 = \text{Re}(y_{e\mu} y_{\mu e})$ for the CLFV process ($\ell = \mu$), while $S_1 = 2|y_e|^2$ and $S_2 = \text{Re}(y_e^2)$ for the CLFC ($\ell = e$), respectively. For the vector interaction in Eq. (4), $X = Z'$ and $g_{Z'} = g' s c$ ($g' s^2$) for the CLFV (CLFC) process. The functions in Eq. (13) are

$$f_1(x) = 0, \quad f_2(x) = 4 - 4x + a_3 x^2, \quad f_3(x) = 2a_4(1-x). \quad (18)$$

In the dipole case, $X = A'$ and $g_{A'} = \mu' m_{A'}$ ($\mu_e m_{A'}$) for the CLFV (CLFC) process, and

$$f_1(x) = 4x, \quad f_2(x) = x(x + 2(r_\ell - r_e)(x - 2)), \quad f_3(x) = 2a_4(1-x). \quad (19)$$

Figures 2, 3, and 4 show the differential cross sections of the bremsstrahlung process for the scalar, vector, and dipole interactions with Eqs. (17), (18), and (19), respectively, as a

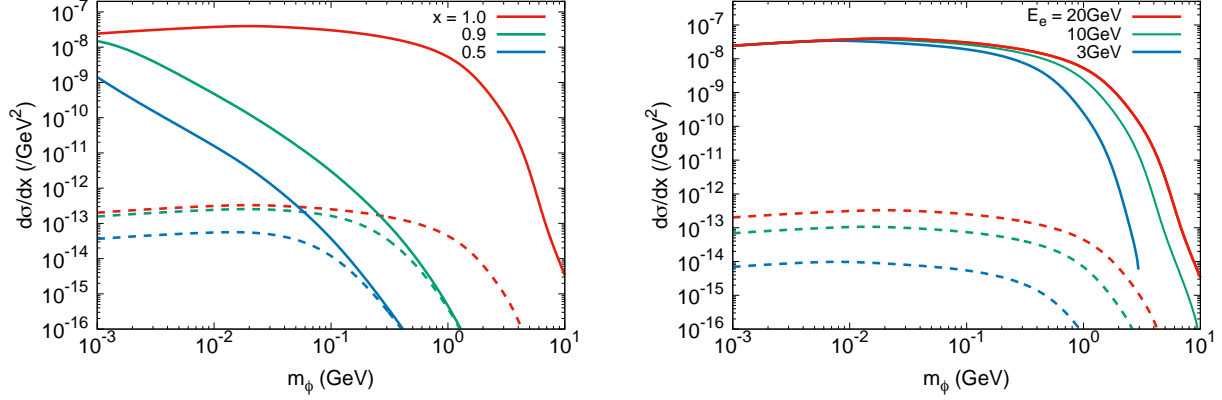


FIG. 2. Differential cross section $d\sigma_{\text{brems}}/dx$ for the scalar interaction. Solid and dashed curves represent the CLFC and CLFV case, respectively, and the coupling constants are taken to be $y_e = y'_{e\mu} = y'_{\mu e} = 10^{-6}$. Left panel: for $x = 1.0$ (red), 0.9 (green) and 0.5 (blue), while fixing E_e as 20 GeV. Right panel: for $E_e = 20$ (red), 10 (green) and 3 (blue) GeV, while fixing x as 1.0.

function of the X boson mass. In the left panels, E_e is fixed to be 20 GeV, and x is taken to be 1.0 (red), 0.9 (green), and 0.5 (blue), respectively. In the right panels, E_e is varied as 20 (red), 10 (green), and 3 (blue) GeV, respectively, and x is fixed to be 1. Solid and dashed curves correspond to the CLFC and CLFV interactions, respectively.

In figure 2, the coupling constants are taken to be $y_e = y'_{e\mu} = y'_{\mu e} = 10^{-6}$ as an illustrating example. In the left panel, the CLFV differential cross sections are much smaller than the CLFC ones with the same x . This is because \tilde{U}_n^ℓ are decreasing functions of η_ℓ , and η_μ is larger than η_e . The CLFC differential cross sections increase by order of magnitudes as x approaches unity because the second term in Eq. (13) is much larger than other terms. These with $x < 1$ also rapidly decrease as m_ϕ becomes large since η_e scales as m_ϕ^2/E_e^2 . On the other hand, the CLFV differential cross sections are rather constant because η_μ scales as m_μ^2/E_e^2 for $m_\phi < m_\mu$. For m_ϕ larger than m_μ , $r_\mu \ll 1$ and $\eta_\mu \simeq \eta_e$, therefore the CLFC and CLFV cross sections asymptotically approach to each other. In the right panel, the CLFC differential cross sections with $x = 1$ are similar to different E_e while the CLFV ones change order of magnitudes. For $x = 1$, Eq. (13) for the CLFC process is approximated as

$$\frac{d\sigma_{\text{brems}}}{dx} \simeq \frac{\alpha^2}{2\pi} \xi \beta_\phi \frac{S_1}{4m_e^2}, \quad (20)$$

where we have used $\tilde{U}_2^e \simeq 1/2\eta_e = E_e^2/2m_e^2$. The effective photon flux is almost constant for $m_\phi < 1$ GeV. Thus, the electron energy dependence only comes from β_ϕ which is almost unity unless close to the threshold. In the CLFV process, on the other hand, the electron energy dependence remains in \tilde{U}_2^e/E_e^2 . From both panels, it can be understood that the main contributions to the signal event come from the CLFC process with $0.9 \lesssim x \lesssim 1$.

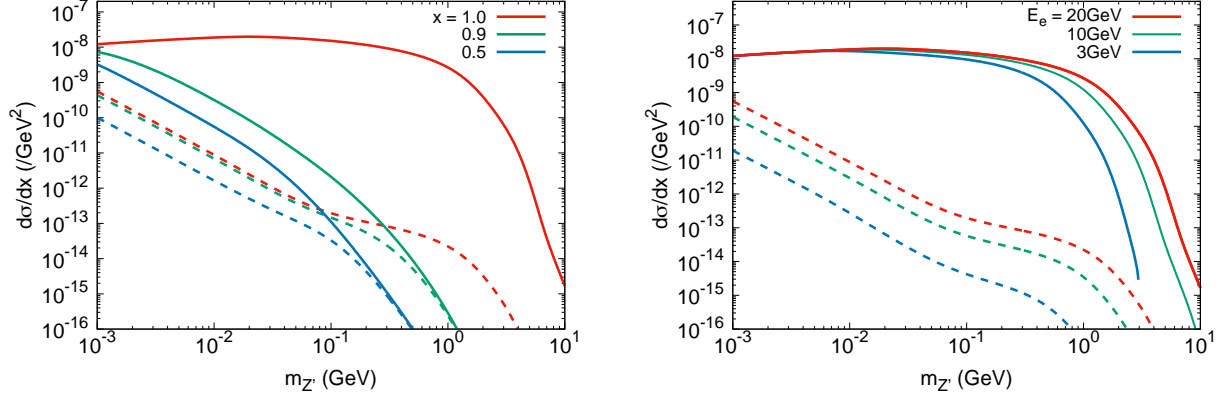


FIG. 3. The same plots as Fig. 2 for the vector interaction. The coupling constants are taken to be $g' = 10^{-6}$ and $\theta = \pi/4$.

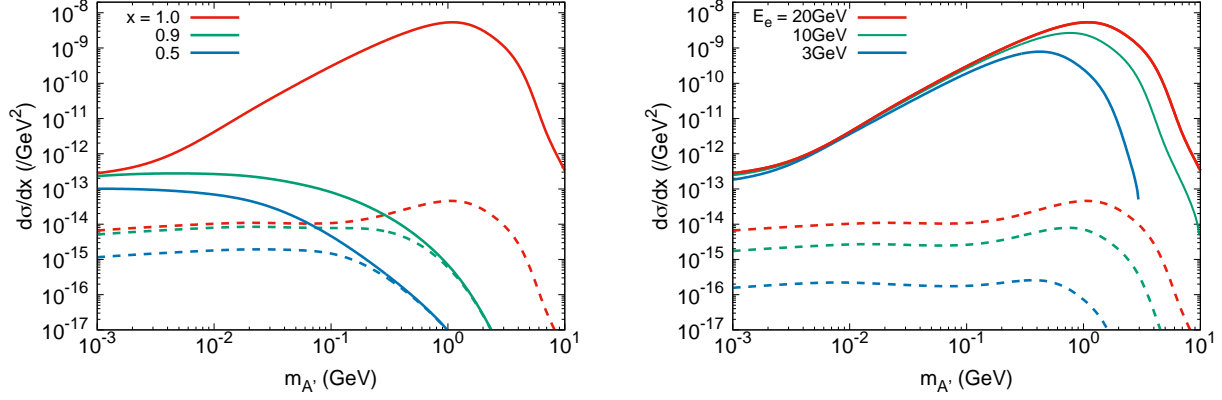


FIG. 4. The same plot as Fig. 2 for the dipole interaction. The coupling constants are taken to be $\mu_e = \mu' = 10^{-6} \text{ GeV}^{-1}$ the for dipole interactions.

Figure 3 shows the same plots with Fig. 2 for the vector interaction. The coupling constant and the mixing angle are fixed to $g' = 10^{-6}$ and $\theta = \pi/4$. Contrary to the scalar interaction case, the CLFV differential cross sections decrease as $m_{Z'}$ increases. This is because $f_2(x)$ in Eq. (18) is dominated by $r_\mu x^2$ for small $m_{Z'}$. The behavior of the CLFC differential cross sections can be understood in the same ways as in the scalar interaction case. Figure 4 also shows the same plots for the dipole interaction. The dipole moments are fixed to $\mu_e = \mu' = 10^{-6} \text{ GeV}^{-1}$. In this case, the differential cross sections are proportional to $m_{A'}^2$. These increase as $m_{A'}$ increases, then goes to zero as the mass reaches to the kinematical threshold. From Figs. 3 and 4, the dominant contributions to the signal events also come from the CLFC differential cross sections with $0.9 \lesssim x \lesssim 1$ for the vector and dipole interaction case, respectively.

target	radiation length X_0 [g/cm ²]	beam energy E_0 [GeV]	total electrons N_e	shield length L_{sh} [m]	decay volume length L_{dec} [m]
^{26.98} ₁₃ Al	24.01	20	1.86×10^{20}	179	204

TABLE I. Setup of the E137 experiment.

B. Number of signal events

The number of the signal events can be calculated by the following formula [31],

$$\begin{aligned}
N = N_e \frac{N_{\text{avo}} X_0}{A} \sum_{\ell=e,\mu} \int_{m_X}^{E_0 - m_\ell} dE_X \int_{E_X + m_\ell}^{E_0} dE_e \int_0^{T_{\text{sh}}} dt \\
\times \left[I_e(E_0, E_e, t) \frac{1}{E_e} \frac{d\sigma_{\text{brems}}}{dx} \Big|_{x=\frac{E_X}{E_e}} e^{-L_{\text{sh}}/L_X} (1 - e^{-L_{\text{dec}}/L_X}) \right] \text{Br}(X \rightarrow e^+e^-), \quad (21)
\end{aligned}$$

where N_e is the number of electrons in the injected beam, $N_{\text{avo}} \simeq 6 \times 10^{23} \text{ mol}^{-1}$ the Avogadro's number, X_0 the radiation length of the target, A the target atomic mass in g/mol, and $T_{\text{sh}} \equiv \rho_{\text{sh}} L_{\text{sh}} / X_0$ with ρ_{sh} being the density of the shield. The length of shield and decay region are denoted as L_{sh} and L_{dec} , respectively. The decay length in laboratory frame and branching ratio of X are denoted by L_X and $\text{Br}(X \rightarrow e^+e^-)$, respectively. The energy distribution of electrons after passing through t radiation lengths in the beam dump is denoted by I_e and given by [56]

$$I_e(E_0, E_e, t) = \frac{1}{E_0} \frac{[\ln(E_0/E_e)]^{bt-1}}{\Gamma(bt)}, \quad (22)$$

where $b = 4/3$. This energy distribution function sharply peaks around $t \simeq 0$ for $E_e = E_0$, and the t integration can diverge. To avoid such divergence, we split the t integration into two parts by a cut t_{cut} , following Ref. [57].

IV. ELECTRON BEAM DUMP CONSTRAINTS

In this section, we show the constraints from electron beam dump experiments, E137 [27], for the scalar, vector, and dipole interactions with CLFV. In the E137 experiment, the electron beam with energy 20 GeV is injected into an aluminium target. The total electrons dumped in the experiment is 1.86×10^{20} . The detector consists of electromagnetic shower counter with dimensions 2 m \times 3 m in the first phase, and 3 m \times 3 m in the second phase. It has 204 m decay region placed at 179 m downstream to the dump². We summarize the setup

² One may consider the produced muon could penetrate the shield and be observed by the detector in beam dump experiments. Using the continuous-slowning-down-approximation range [58], the range for the muon to be stopped is estimated at $\sim 50\text{m}$ at most for the E137 experiment. The range is 1/3 times shorter than the shield length. Therefore, the produced muon would be stopped in the shield.

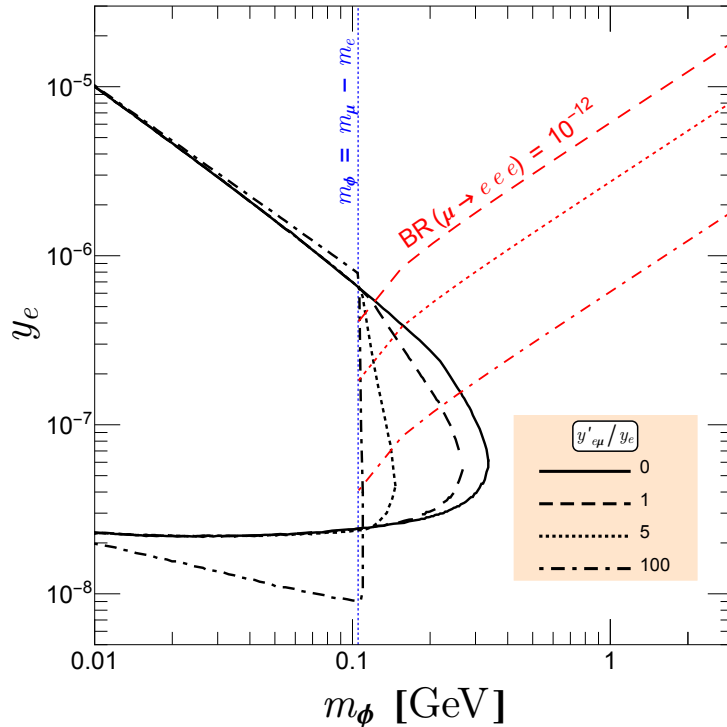


FIG. 5. Exclusion region from the E137 experiment for the scalar interaction. The CLFV coupling is taken to $y'_{e\mu}/y_e = 0$ (solid), 1 (dashed), 5 (dotted) and 100 (dot-dashed). Red curves represent the constraints from $\mu \rightarrow eee$, and blue vertical line corresponds to $m_\phi = m_\mu - m_e$.

of the E137 experiment in Tab. I. In order to take into account the geometrical acceptance, we set θ_{\max} in Eq. (B1) as $\theta_{\max} = 0.00392$ rad. The E137 collaboration reported null results for the energy above 3 GeV in the search for axion-like particles, so that we regard the regions predicting $N > 3$ events as the 95% C.L. exclusion regions and set the lower cut of 3 GeV on the E_X integral in Eq. (21).

Figure 5 shows the exclusion regions in m_ϕ - y_e plane at 95% C.L. from the E137 for the scalar case. For simplicity, we assumed $y'_{e\mu} = y'_{\mu e}$ and $y_e, y_{e\mu}$ are real. Solid, dashed, dotted and dot-dashed curves correspond to $y'_{e\mu}/y_e = 0, 1, 5$ and 100, respectively. Among them, $y'_{e\mu}/y_e = 0$ (the solid curve) corresponds to the case of no CLFV coupling, and we find that the E137 excludes large parameter regions below $m_\phi = 0.35$ GeV. For the cases of nonzero $y'_{e\mu}$, there are strong constraints from CLFV decays of the muon. The regions above the red curves are excluded by $\mu \rightarrow eee$, while most regions of the left side of the blue vertical line are excluded by $\mu \rightarrow e\phi$. The upper bounds of these decay branching ratios are listed in Table II, and the partial widths of these CLFV decays are given in Appendix C. Note that constraints from $\mu \rightarrow e\gamma$ are weaker than those from $\mu \rightarrow eee$ since the decay width of $\mu \rightarrow e\gamma$ is suppressed by the electromagnetic coupling and a loop factor in comparison with

$\text{Br}(\mu \rightarrow eee)$	$\text{Br}(\mu \rightarrow eX)$		
$m_X > m_\mu - m_e$	$13 < m_X < 80$	$47.8 < m_X < 95.1$	$98.1 < m_X < 103.5$
$< 1.0 \times 10^{-12}$ [59]	$\lesssim 5.8 \times 10^{-5}$ [60]	$\lesssim 10^{-5}$ [61]	$\lesssim 2 \times 10^{-4}$ [62]

TABLE II. Upper bounds on the branching ratios of $\mu \rightarrow eee$ and $\mu \rightarrow eX$. Masses are in MeV.

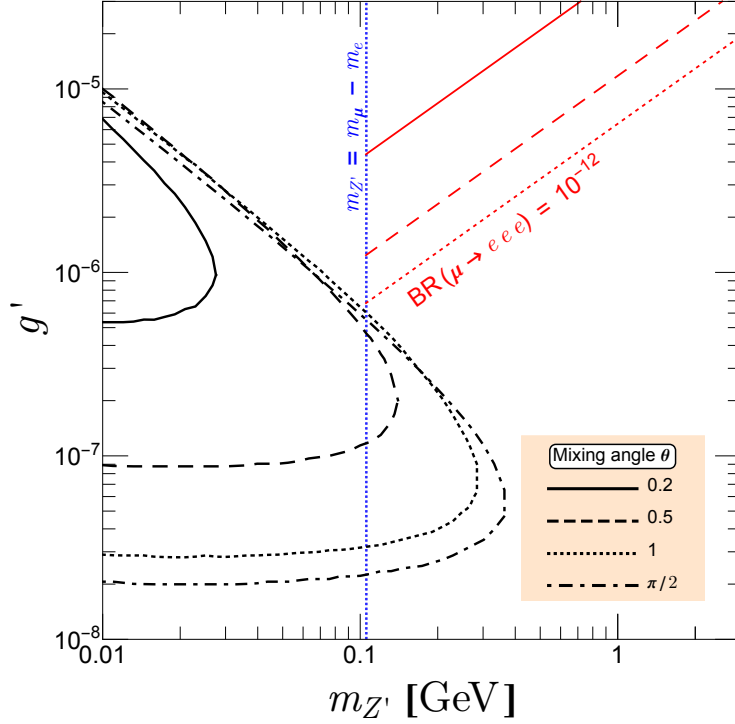


FIG. 6. The same plots as Fig. 5 for the vector interaction. The mixing angle is taken to 0.2 (solid), 0.5 (dashed), 1 (dotted) and $\pi/2$ (dot-dashed), respectively.

that of $\mu \rightarrow eee$. As can be seen from the figure, most of the parameter regions are excluded by these constraints. Nevertheless, we find that our 95% C.L. limit further excludes the parameter regions unconstrained by $\mu \rightarrow eee$ and $\mu \rightarrow e\phi$. The exclusion region shifts to lighter m_ϕ as $y'_{e\mu}/y_e$ increases. As we explained in Sec. III, the differential cross sections are mainly determined by the CLFC ones for $y'_{e\mu} < 10$. Therefore, in this case, the effects of the flavor violating couplings appear only in the total decay width. Once the threshold of $\phi \rightarrow e\mu$ opens, the decay length and branching ratio of $\phi \rightarrow ee$ become smaller. Then, the expected number of the signal events reduces, resulting in the exclusion regions shown in Figure 5. For $y'_{e\mu} = 100$, contributions from the CLFV differential cross sections are not negligible, making the exclusion regions wider especially in the small y_e regions. Such a large $y'_{e\mu}$, however, makes the decay length and the branching ratio so small that no signal events are expected above the threshold of $\mu \rightarrow e\phi$.

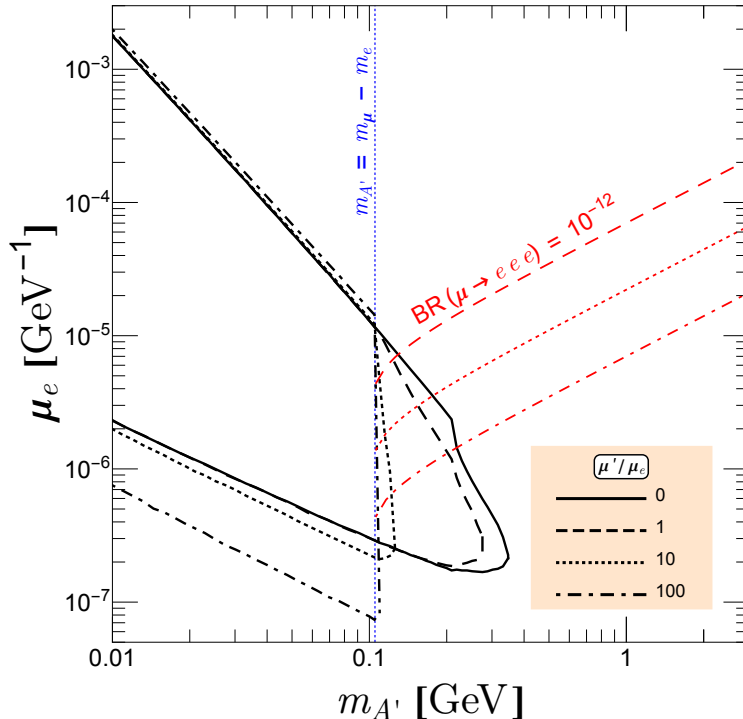


FIG. 7. The same plots as Fig. 5 for the dipole interaction. The dipoles are taken to $\mu'/\mu_e = 0$ (solid), 1 (dashed), 10 (dotted) and 100 (dot-dashed), respectively.

Figure 6 shows the exclusion plot in $m_{Z'}-g'$ plane for the vector interaction. The mixing angle is varied as $\theta = 0.2$ (solid), 0.5 (dashed), 1 (dotted) and $\pi/2$ (dot-dashed), respectively. The red and blue curves represent the same constraints as in Fig. 5. In contrast to the case of the scalar interaction, the exclusion regions become wider as the CLFV mixing becomes large. This is because a nonzero θ induces interactions between Z' and electrons³, increasing the production cross sections and the branching ratio of $Z' \rightarrow ee$. For $\theta > 0.5$, the constraint from E137 experiment excludes the parameter regions for $m_{Z'} > m_{\mu} + m_e$, which are not constrained by $\mu \rightarrow eee$ and $\mu \rightarrow eZ'$. When $\theta = \pi/2$, the interaction to muon vanishes and the exclusion region coincides with that for the minimal $U(1)_{L_e-L_\tau}$ model [33].

Figure 7 is the same plot as Fig. 5 and 6 for the dipole interaction in $m_{A'}-\mu_e$ plane. The CLFV dipole is taken to $\mu'/\mu_e = 0$ (solid), 1 (dashed), 10 (dotted) and 100 (dot-dashed), respectively. In this case, the constraint from the E137 experiment also excludes the parameter region below the $\mu \rightarrow eee$ limit. The behavior of the exclusion region is similar to the scalar interaction case.

³ Even in the case of $\theta = 0$, interactions between Z' and electrons arise at one loop level, which yields narrow exclusion regions around $m_{Z'} = 0.001-0.003$ GeV [33].

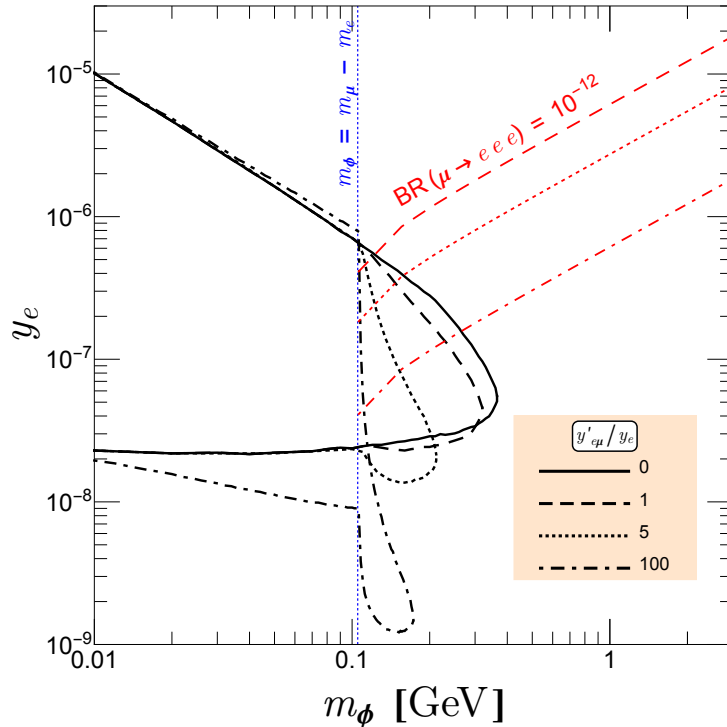


FIG. 8. Presumed exclusion region to $\phi \rightarrow ee$, $e\mu$, $\mu\mu$ decays in the E137 experiment for the scalar interaction. The parameters are taken as $y'_{e\mu}/y_e = 0$ (solid), 1 (dashed), 5 (dotted) and 100 (dot-dashed).

V. FLAVOR VIOLATING DECAY SIGNAL

In the previous section, we have only considered the CLFC decay of $X \rightarrow ee$ as the signal of the vector and scalar boson, based on the setup and analyses of the E137 experiment. Under the presence of the CLFV interactions, the light bosons can decay into $e\bar{\mu}$ and $\bar{e}\mu$ above its kinematical threshold. This decay mode is a smoking gun signature of CLFV interactions in the dark sector. Searches for these decays will bring further information on the CLFV couplings.

To illustrate the impact of the CLFV decay searches, we have demonstrated analyses for the scalar CLFV decays with the setup of the E137 experiment in Table. I. Figure 8 shows presumed excluded regions with 95% C.L. for $\phi \rightarrow ee$, $e\mu$, $\mu\mu$. The solid, dashed, dotted and dot-dashed curves correspond to $y'_{e\mu}/y_e = 0, 1, 5$ and 100, respectively. Compared with Fig. 5, smaller coupling and larger mass regions can be excluded above the $e\mu$ threshold. This is because, for $m_\phi \geq m_e + m_\mu$ ($2m_\mu$), the decay branch of $\phi \rightarrow e\mu$ ($\mu\mu$) opens, and the decay length of the light boson shortens. The smaller coupling is, therefore, preferred to reach the detector of the E137 experiment. Since these regions cannot be excluded only

by analyzing the ee decay search, the CLFV couplings can be further constrained in these regions. Thus, it is important to search for not only the CLFC decays but also the CLFV decays as signals in future beam dump experiments. The FASER experiment [63–65], which will start next year, will be able to perform the searches for the dark photon decay into $e\mu$ pairs. Theoretical analyses will be shown in [66].

VI. SUMMARY

We have studied the constraints from the electron beam dump experiment taking into account the charged lepton flavor violating interactions. The scalar, vector, and dipole type interactions are considered and the excluded regions have been derived for the search for $X \rightarrow ee$. We have found that the parameter regions unconstrained by $\mu \rightarrow eee$ and $\mu \rightarrow eX$ can be excluded for three interactions. The exclusion regions depend on the CLFV and CLFC couplings as well as the boson mass, and new bounds can be derived when the ratios of the CLFV coupling to the CLFC one are $\lesssim 100$. For the illustrative purpose, we have also derived the presumed excluded region for the search of $\phi \rightarrow ee, e\mu, \mu\mu$ decays in the same setup with the E137 experiment. It has been found that the excluded regions can be extended and the CLFV couplings can be further constrained in those regions. Such searches and analyses for the CLFV decays will be important to new physics searches in future experiments.

ACKNOWLEDGMENTS

This work was supported by JSPS KAKENHI Grant Number JP20K04004 [YT], JP18H01210 [TA, TS], JP18K03651, and MEXT KAKENHI Grant Number JP18H05543 [TS].

Appendix A: Effective photon flux

The effective photon flux ξ produced by an atom with mass number A and atomic number Z is defined by [31]

$$\xi = \int_{t_{\min}}^{t_{\max}} dt \frac{t - t_{\min}}{t^2} G_2(t) , \quad (\text{A1})$$

where $t_{\min} = (m_X^2/2E_e)^2$ and $t_{\max} = m_X^2$. The electric form factor $G_2(t)$ is given by elastic and inelastic components,

$$G_2(t) = G_{2,\text{el}} + G_{2,\text{inel}} . \quad (\text{A2})$$

The elastic electric form factor is given by

$$G_{2,\text{el}} = \left(\frac{a^2 t}{1 + a^2 t} \right)^2 \left(\frac{1}{1 + \frac{t}{d}} \right)^2 Z^2, \quad (\text{A3})$$

where $a = 111Z^{-1/3}/m_e$ and $d = 0.164 \text{ GeV}^2 A^{-2/3}$. The inelastic electric form factor is given by

$$G_{2,\text{in}} = \left(\frac{a'^2 t}{1 + a'^2 t} \right)^2 \left(\frac{1 + \frac{t}{4m_p^2}(\mu_p^2 - 1)}{(1 + \frac{t}{0.71 \text{ GeV}^2})^4} \right)^2 Z, \quad (\text{A4})$$

where $a' = 773Z^{-2/3}/m_e$, m_p is the proton mass and $\mu_p = 2.79$.

The electric form factor is dominated by the elastic one in our study, thus it scales by Z^2 . See [31] for more detail.

Appendix B: Function \tilde{U}_n^ℓ

The functions \tilde{U}_n^ℓ ($n = 1-4$) are defined by

$$\tilde{U}_n^\ell = \int_0^{\theta_{\text{max}}} \frac{\sin \theta}{[\theta^2 + \eta_\ell(x)]^n} d\theta, \quad (\text{B1})$$

where θ_{max} is the maximal angle determined by angular acceptance of the detector, and $\eta_\ell(x)$ is given in Eq. (14). For the small angle θ_{max} , \tilde{U}_n^ℓ can be approximated by the following formulae :

$$\begin{aligned} \tilde{U}_1^\ell &\simeq \frac{1}{2} \log \left(\frac{\eta_\ell + \theta_{\text{max}}^2}{\eta_\ell} \right) + \frac{1}{12} \left(\eta_\ell \log \left(\frac{\eta_\ell + \theta_{\text{max}}^2}{\eta_\ell} \right) - \theta_{\text{max}}^2 \right) \\ &\quad + \frac{1}{480} \left(2\eta_\ell^2 \log \left(\frac{\eta_\ell + \theta_{\text{max}}^2}{\eta_\ell} \right) - 2\eta_\ell \theta_{\text{max}}^2 + \theta_{\text{max}}^4 \right), \end{aligned} \quad (\text{B2a})$$

$$\begin{aligned} \tilde{U}_2^\ell &\simeq \frac{\theta_{\text{max}}^2}{2\eta_\ell(\eta_\ell + \theta_{\text{max}}^2)} + \frac{1}{12} \left(-\frac{\eta_\ell}{\eta_\ell + \theta_{\text{max}}^2} - \log \left(\frac{\eta_\ell + \theta_{\text{max}}^2}{\eta_\ell} \right) + 1 \right) \\ &\quad + \frac{1}{120} \left(\frac{(2\eta_\ell + \theta_{\text{max}}^2)\theta_{\text{max}}^2}{2(\eta_\ell + \theta_{\text{max}}^2)} - \eta_\ell \log \left(\frac{\eta_\ell + \theta_{\text{max}}^2}{\eta_\ell} \right) \right), \end{aligned} \quad (\text{B2b})$$

$$\begin{aligned} \tilde{U}_3^\ell &\simeq \frac{(2\eta_\ell + \theta_{\text{max}}^2)\theta_{\text{max}}^2}{4\eta_\ell^2(\eta_\ell + \theta_{\text{max}}^2)^2} - \frac{\theta_{\text{max}}^4}{24\eta_\ell(\eta_\ell + \theta_{\text{max}}^2)^2} \\ &\quad + \frac{1}{120} \left(\frac{1}{2} \log \left(\frac{\eta_\ell + \theta_{\text{max}}^2}{\eta_\ell} \right) - \frac{(2\eta_\ell + 3\theta_{\text{max}}^2)\theta_{\text{max}}^2}{4(\eta_\ell + \theta_{\text{max}}^2)^2} \right), \end{aligned} \quad (\text{B2c})$$

$$\tilde{U}_4^\ell \simeq \frac{(3\eta_\ell^2 + 3\eta_\ell\theta_{\text{max}}^2 + \theta_{\text{max}}^4)\theta_{\text{max}}^2}{6\eta_\ell^3(\eta_\ell + \theta_{\text{max}}^2)^3} - \frac{(3\eta_\ell + \theta_{\text{max}}^2)\theta_{\text{max}}^4}{72\eta_\ell^2(\eta_\ell + \theta_{\text{max}}^2)^3} + \frac{\theta_{\text{max}}^6}{720\eta_\ell(\eta_\ell + \theta_{\text{max}}^2)^3}. \quad (\text{B2d})$$

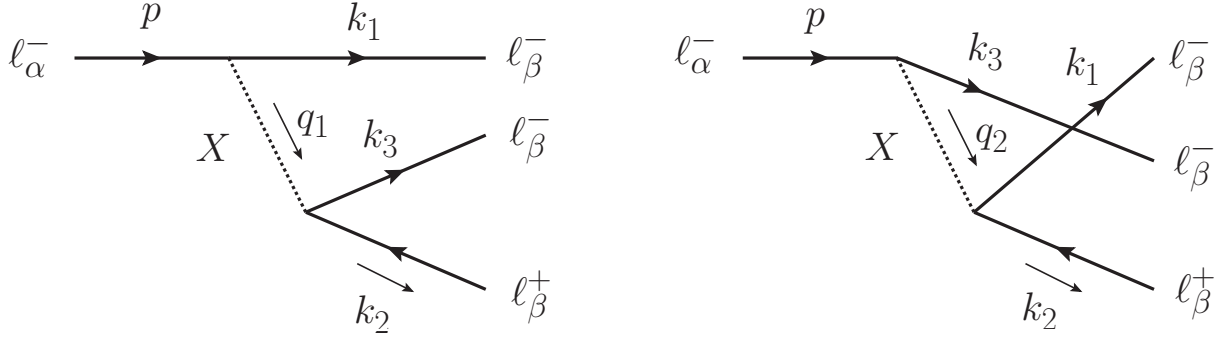


FIG. 9. Feynman diagrams of the process $\ell_\alpha^- \rightarrow \ell_\beta^- \ell_\beta^- \ell_\beta^+$, in which ℓ_α^- represents the SM charged lepton and $X = \phi, Z', A'$.

Appendix C: Widths of CLFV decays of muons

We here discuss the experimental limits on the CLFV decays of the muon. The CLFV is tightly constrained by the rare muon decays, i.e., $\mu \rightarrow e\gamma$ and $\mu \rightarrow eee$. The current strongest limits on the branching ratio of $\mu \rightarrow e\gamma$ is given by MEG [50] as $\text{BR}(\mu \rightarrow e\gamma) < 4.2 \times 10^{-13}$. On the other hand, the strongest limits of $\mu \rightarrow eee$ is given by SINDRUM [59] as $\text{BR}(\mu \rightarrow eee) < 10^{-12}$. Though, the constraint on $\text{BR}(\mu \rightarrow e\gamma)$ is stronger than that on $\text{BR}(\mu \rightarrow eee)$, the decay width of $\mu \rightarrow e\gamma$ is suppressed by the electromagnetic coupling and a loop factor in comparison with that of $\mu \rightarrow eee$. As a result, usually, the bound on CLFV couplings from $\mu \rightarrow eee$ is stronger than that from $\mu \rightarrow e\gamma$. We, therefore, take into account only the constraint from $\mu \rightarrow eee$ for $m_X > m_\mu - m_e$ in this work. For $m_X < m_\mu - m_e$, muons can decay into the light bosons. The TWIST collaboration [60] gives the limits on the branching ratio of $\mu \rightarrow eX$ as $\text{BR}(\mu \rightarrow eX) < 5.8 \times 10^{-5}$ for $m_X = 13\text{-}80$ MeV. The PIENU collaboration [61] also gives the upper limit as $\text{BR}(\mu \rightarrow eX) \lesssim 10^{-5}\text{-}10^{-4}$ for $m_X = 47.8\text{-}95.1$ MeV. Moreover, Ref. [62] gives the upper limit as $\text{BR}(\mu \rightarrow eX) < 2 \times 10^{-4}$ for $m_X = 98.1\text{-}103.5$ MeV. These limits give much more severe constraints on the CLFV coupling than that from the electron beam dump, and then we focus on the region where the light boson is heavier than $m_\mu - m_e$.

The partial decay width of $\ell_\alpha^- \rightarrow \ell_\beta^- \ell_\beta^- \ell_\beta^+$ is given by

$$\Gamma = \frac{1}{(8\pi m_\alpha)^3} \int_{s_{12}^{\min}}^{s_{12}^{\max}} ds_{12} \int_{s_{23}^{\min}}^{s_{23}^{\max}} ds_{23} \frac{1}{2} \sum_{\text{spin}} |M|^2, \quad (\text{C1})$$

where $s_{12} = (p - k_3)^2$ and $s_{23} = (p - k_1)^2$. The integral ranges of s_{12} and s_{23} are given by

$$s_{23}^{\max} = (\hat{E}_2 + \hat{E}_3)^2 - (\hat{P}_2 - \hat{P}_3)^2, \quad (\text{C2a})$$

$$s_{23}^{\min} = (\hat{E}_2 + \hat{E}_3)^2 - (\hat{P}_2 + \hat{P}_3)^2, \quad (\text{C2b})$$

$$s_{12}^{\max} = (m_\alpha - m_\beta)^2, \quad (\text{C2c})$$

$$s_{12}^{\min} = 4m_\beta^2, \quad (\text{C2d})$$

where

$$\hat{E}_2 = \frac{1}{2\sqrt{s_{12}}}(m_\alpha^2 - s_{12} - m_\beta^2), \quad (\text{C3a})$$

$$\hat{E}_3 = \frac{\sqrt{s_{12}}}{2}, \quad (\text{C3b})$$

$$\hat{P}_2 = \frac{1}{2}\sqrt{s_{12} - 2(m_\alpha^2 + m_\beta^2) + \frac{(m_\alpha^2 - m_\beta^2)^2}{s_{12}}}, \quad (\text{C3c})$$

$$\hat{P}_3 = \frac{1}{2}\sqrt{s_{12} - 4m_\beta^2}. \quad (\text{C3d})$$

The amplitude is written as

$$\frac{1}{2} \sum_{\text{spin}} |\mathcal{M}|^2 = \frac{C^2}{2} [P_X^2(s_{23}) M_1^2 + P_X^2(s_{12}) M_2^2 - 2P_X(s_{23})P_X(s_{12}) \text{Re}[M_3^2]] , \quad (\text{C4})$$

where $P_X(s_{23(12)}) = (s_{23(12)} - m_X^2)^{-1}$, $X = \phi, Z', A'$, and $C = y_e y'_{e\mu}$, $g' s^3 c$ and $\mu_e \mu'$ for the scalar, the vector and the dipole interaction, respectively. For the scalar interaction,

$$M_1^2 = -4(s_{23} - 4m_\beta^2)(s_{23} - (m_\alpha + m_\beta)^2), \quad (\text{C5a})$$

$$M_2^2 = -4(s_{12} - 4m_\beta^2)(s_{12} - (m_\alpha + m_\beta)^2), \quad (\text{C5b})$$

$$M_3^2 = 2s_{12}s_{23} + 4m_\beta(m_\alpha + m_\beta)(s_{12} + s_{23}) - 2m_\beta(m_\alpha + m_\beta)(5m_\beta^5 + 2m_\alpha m_\beta + m_\alpha^2), \quad (\text{C5c})$$

for the vector interaction,

$$M_1^2 = -8\{2s_{12}^2 + s_{23}^2 + 2s_{12}s_{23} - (m_\alpha - m_\beta)^2 s_{23} - 2(m_\alpha^2 + 3m_\beta^2)s_{12} + 2m_\beta^2(m_\alpha + m_\beta)^2\}, \quad (\text{C6a})$$

$$M_2^2 = -8\{2s_{23}^2 + s_{12}^2 + 2s_{12}s_{23} - (m_\alpha - m_\beta)^2 s_{12} - 2(m_\alpha^2 + 3m_\beta^2)s_{23} + 2m_\beta^2(m_\alpha + m_\beta)^2\}, \quad (\text{C6b})$$

$$M_3^2 = 8(s_{12} + s_{23} + m_\beta(m_\alpha + m_\beta))(s_{12} + s_{23} - m_\alpha^2 + m_\alpha m_\beta - 2m_\beta^2), \quad (\text{C6c})$$

and for the dipole interaction,

$$M_1^2 = -4s_{23} \left\{ s_{23}^3 + 4(s_{12} + s_{23})s_{12}s_{23} - (m_\alpha - m_\beta)^2 s_{23}^2 \right. \\ \left. - 4(m_\alpha^2 + 3m_\beta^2)s_{12}s_{23} + 8m_\beta^2(m_\alpha + m_\beta)^2 s_{23} - 4m_\beta^2(m_\alpha^2 - m_\beta^2)^2 \right\} , \quad (\text{C7a})$$

$$M_2^2 = -4s_{12} \left\{ s_{12}^3 + 4(s_{12} + s_{23})s_{12}s_{23} - (m_\alpha - m_\beta)^2 s_{12}^2 \right. \\ \left. - 4(m_\alpha^2 + 3m_\beta^2)s_{12}s_{23} + 8m_\beta^2(m_\alpha + m_\beta)^2 s_{12} - 4m_\beta^2(m_\alpha^2 - m_\beta^2)^2 \right\} , \quad (\text{C7b})$$

$$M_3^2 = 2 \left\{ 2(s_{12}^2 + s_{23}^2)s_{12}s_{23} + 5s_{12}^2 s_{23}^2 - 2(m_\alpha^2 + 3m_\beta^2)(s_{12} + s_{23})s_{12}s_{23} \right. \\ \left. + m_\beta(m_\alpha + m_\beta)(3m_\alpha^2 + 2m_\alpha m_\beta + 11m_\beta^2)s_{12}s_{23} \right. \\ \left. - 2m_\beta^2(m_\alpha^2 - m_\beta^2)^2(s_{12} + s_{23}) - 4m_\beta^3(m_\alpha + m_\beta)(m_\alpha^2 - m_\beta^2)^2 \right\} , \quad (\text{C7c})$$

where m_α stands for the mass of the α flavor charged lepton.

The partial width of the muon decay into an electron and a light boson is given by

$$\Gamma(\mu \rightarrow e\phi) = \frac{\lambda_{e\mu}^2}{16\pi} m_\mu \lambda \left(\frac{m_e^2}{m_\mu^2}, \frac{m_\phi^2}{m_\mu^2} \right) \left\{ 1 + 2\frac{m_e}{m_\mu} + \frac{m_e^2 - m_\phi^2}{m_\mu^2} \right\} , \quad (\text{C8})$$

$$\Gamma(\mu \rightarrow eZ') = \frac{(g'sc)^2}{16\pi} m_\mu \lambda \left(\frac{m_e^2}{m_\mu^2}, \frac{m_{Z'}^2}{m_\mu^2} \right) \frac{m_\mu^2}{m_{Z'}^2} \\ \times \left\{ \left(1 - \frac{m_e^2}{m_\mu^2} \right)^2 - \frac{m_{Z'}^4}{m_\mu^4} + \left(1 - 6\frac{m_e}{m_\mu} + \frac{m_e^2 - m_{Z'}^2}{m_\mu^2} \right) \frac{m_{Z'}^2}{m_\mu^2} \right\} , \quad (\text{C9})$$

$$\Gamma(\mu \rightarrow eA') = \frac{(\mu'm_\mu)^2}{16\pi} m_\mu \lambda \left(\frac{m_e^2}{m_\mu^2}, \frac{m_{A'}^2}{m_\mu^2} \right) \\ \times \left[2 \left\{ \left(1 - \frac{m_e^2}{m_\mu^2} \right)^2 - \frac{m_{A'}^4}{m_\mu^4} \right\} - \left(1 + 6\frac{m_e}{m_\mu} + \frac{m_e^2 - m_{A'}^2}{m_\mu^2} \right) \frac{m_{A'}^2}{m_\mu^2} \right] , \quad (\text{C10})$$

for the scalar, vector, and dipole interaction, respectively, and $\lambda(a, b)$ is the Kallen function given in Eq. (8).

-
- [1] D. Tucker-Smith and N. Weiner, Phys. Rev. D **64**, 043502 (2001), hep-ph/0101138.
 - [2] C. Boehm and P. Fayet, Nucl. Phys. B **683**, 219 (2004), hep-ph/0305261.
 - [3] M. Pospelov, A. Ritz, and M. B. Voloshin, Phys. Lett. B **662**, 53 (2008), 0711.4866.
 - [4] E. Izaguirre, G. Krnjaic, P. Schuster, and N. Toro, Phys. Rev. Lett. **115**, 251301 (2015), 1505.00011.
 - [5] S. Knapen, T. Lin, and K. M. Zurek, Phys. Rev. D **96**, 115021 (2017), 1709.07882.
 - [6] P. J. Fitzpatrick, H. Liu, T. R. Slatyer, and Y.-D. Tsai (2020), 2011.01240.
 - [7] M. Duerr, T. Ferber, C. Garcia-Cely, C. Hearty, and K. Schmidt-Hoberg, JHEP **04**, 146 (2021), 2012.08595.

- [8] S. Baek, N. G. Deshpande, X. G. He, and P. Ko, Phys. Rev. D **64**, 055006 (2001), hep-ph/0104141.
- [9] M. Pospelov, Phys. Rev. D **80**, 095002 (2009), 0811.1030.
- [10] W. Altmannshofer, S. Gori, M. Pospelov, and I. Yavin, Phys. Rev. Lett. **113**, 091801 (2014), 1406.2332.
- [11] M. Escudero, D. Hooper, G. Krnjaic, and M. Pierre, JHEP **03**, 071 (2019), 1901.02010.
- [12] M. Escudero and S. J. Witte, Eur. Phys. J. C **80**, 294 (2020), 1909.04044.
- [13] M. Escudero Abenza, JCAP **05**, 048 (2020), 2001.04466.
- [14] T. Araki, K. Asai, K. Honda, R. Kasuya, J. Sato, T. Shimomura, and M. J. S. Yang (2021), 2103.07167.
- [15] K. Ioka and K. Murase, PTEP **2014**, 061E01 (2014), 1404.2279.
- [16] K. C. Y. Ng and J. F. Beacom, Phys. Rev. D **90**, 065035 (2014), [Erratum: Phys.Rev.D 90, 089904 (2014)], 1404.2288.
- [17] M. Ibe and K. Kaneta, Phys. Rev. D **90**, 053011 (2014), 1407.2848.
- [18] T. Araki, F. Kaneko, Y. Konishi, T. Ota, J. Sato, and T. Shimomura, Phys. Rev. D **91**, 037301 (2015), 1409.4180.
- [19] A. Kamada and H.-B. Yu, Phys. Rev. D **92**, 113004 (2015), 1504.00711.
- [20] A. DiFranzo and D. Hooper, Phys. Rev. D **92**, 095007 (2015), 1507.03015.
- [21] T. Araki, F. Kaneko, T. Ota, J. Sato, and T. Shimomura, Phys. Rev. D **93**, 013014 (2016), 1508.07471.
- [22] S. Mohanty, A. Narang, and S. Sadhukhan, JCAP **03**, 041 (2019), 1808.01272.
- [23] J. A. Carpio, K. Murase, I. M. Shoemaker, and Z. Tabrizi (2021), 2104.15136.
- [24] F. Bergsma et al. (CHARM), Phys. Lett. B **157**, 458 (1985).
- [25] A. Konaka et al., Phys. Rev. Lett. **57**, 659 (1986).
- [26] E. M. Riordan et al., Phys. Rev. Lett. **59**, 755 (1987).
- [27] J. D. Bjorken, S. Ecklund, W. R. Nelson, A. Abashian, C. Church, B. Lu, L. W. Mo, T. A. Nunamaker, and P. Rassmann, Phys. Rev. D **38**, 3375 (1988).
- [28] A. Bross, M. Crisler, S. H. Pordes, J. Volk, S. Errede, and J. Wrbanek, Phys. Rev. Lett. **67**, 2942 (1991).
- [29] M. Davier and H. Nguyen Ngoc, Phys. Lett. B **229**, 150 (1989).
- [30] S. N. Gninenko, Phys. Lett. B **713**, 244 (2012), 1204.3583.
- [31] J. D. Bjorken, R. Essig, P. Schuster, and N. Toro, Phys. Rev. D **80**, 075018 (2009), 0906.0580.
- [32] S. Andreas, C. Niebuhr, and A. Ringwald, Phys. Rev. D **86**, 095019 (2012), 1209.6083.
- [33] M. Bauer, P. Foldenauer, and J. Jaeckel, JHEP **07**, 094 (2018), 1803.05466.
- [34] M. Fabbrichesi, E. Gabrielli, and G. Lanfranchi (2020), 2005.01515.

- [35] A. Caputo, C. A. J. O'Hare, A. J. Millar, and E. Vitagliano (2021), 2105.04565.
- [36] M. W. Winkler, Phys. Rev. D **99**, 015018 (2019), 1809.01876.
- [37] S. Kanemura, T. Moroi, and T. Tanabe, Phys. Lett. B **751**, 25 (2015), 1507.02809.
- [38] Y. Sakaki and D. Ueda, Phys. Rev. D **103**, 035024 (2021), 2009.13790.
- [39] K. Asai, T. Moroi, and A. Niki (2021), 2104.00888.
- [40] K. Asai, S. Iwamoto, Y. Sakaki, and D. Ueda (2021), 2105.13768.
- [41] J. Heeck, Phys. Lett. B **758**, 101 (2016), 1602.03810.
- [42] W. Altmannshofer, C.-Y. Chen, P. S. Bhupal Dev, and A. Soni, Phys. Lett. B **762**, 389 (2016), 1607.06832.
- [43] S. Iguro, Y. Omura, and M. Takeuchi, JHEP **09**, 144 (2020), 2002.12728.
- [44] H. Davoudiasl, R. Marcarelli, N. Miesch, and E. T. Neil (2021), 2105.05866.
- [45] R. Foot, Mod.Phys.Lett. **A6**, 527 (1991).
- [46] X. He, G. C. Joshi, H. Lew, and R. Volkas, Phys.Rev. **D43**, 22 (1991).
- [47] R. Foot, X. G. He, H. Lew, and R. R. Volkas, Phys. Rev. D **50**, 4571 (1994), hep-ph/9401250.
- [48] J. L. Diaz-Cruz and J. J. Toscano, Phys. Rev. D **62**, 116005 (2000), hep-ph/9910233.
- [49] E. Arganda, A. M. Curiel, M. J. Herrero, and D. Temes, Phys. Rev. D **71**, 035011 (2005), hep-ph/0407302.
- [50] A. M. Baldini et al. (MEG), Eur. Phys. J. C **76**, 434 (2016), 1605.05081.
- [51] B. Aubert et al. (BaBar), Phys. Rev. Lett. **104**, 021802 (2010), 0908.2381.
- [52] T. Nomura, H. Okada, and Y. Uesaka, JHEP **01**, 016 (2021), 2005.05527.
- [53] C. F. von Weizsacker, Z. Phys. **88**, 612 (1934).
- [54] E. J. Williams, Matematisk-fysiske Meddelelser **13**, 1 (1935).
- [55] K. J. Kim and Y.-S. Tsai, Phys. Rev. D **8**, 3109 (1973).
- [56] Y.-S. Tsai, Phys. Rev. D **34**, 1326 (1986).
- [57] S. Andreas, Ph.D. thesis, Hamburg U. (2013).
- [58] P. Zyla et al. (Particle Data Group), PTEP **2020**, 083C01 (2020).
- [59] U. Bellgardt et al. (SINDRUM), Nucl. Phys. B **299**, 1 (1988).
- [60] R. Bayes et al. (TWIST), Phys. Rev. D **91**, 052020 (2015), 1409.0638.
- [61] A. Aguilar-Arevalo et al. (PIENU), Phys. Rev. D **101**, 052014 (2020), 2002.09170.
- [62] S. E. Derenzo, Phys. Rev. **181**, 1854 (1969).
- [63] J. L. Feng, I. Galon, F. Kling, and S. Trojanowski, Phys. Rev. D **97**, 035001 (2018), 1708.09389.
- [64] J. L. Feng, I. Galon, F. Kling, and S. Trojanowski, Phys. Rev. D **97**, 055034 (2018), 1710.09387.
- [65] A. Ariga et al. (FASER), Phys. Rev. D **99**, 095011 (2019), 1811.12522.
- [66] T. Araki, K. Asai, H. Otono, T. Shimomura, and Y. Takubo, work in progress.